Morphological Algorithms for Processing Tickets by Hand Held Assay

Mingkai Hsueh[1] Antonio Plaza[1,2] Jing Wang[1] Su Wang[1] Wei-min Liu[1] Hsuan Ren[3] Chein-I Chang[1]
Janet L. Jensen[4] James O. Jensen[4] Matthew A. Odom[5] Ryen Hydutsky[5] Harlan Knapp[5] Ray Yin[5]

[1]Remote Sensing Signal and Image Processing Laboratory
Department of Computer Science and Electrical Engineering
University of Maryland Baltimore County, Baltimore, MD 21250
[2]Computer Science Department, University of Extremadura
Avda. de la Universidad s/n,10.071 Caceres, SPAIN
[3]Center for Space and Remote Sensing Research
Graduate Institute of Space Science
Department of Computer Science and Information Engineering
National Central University, Chungli, Taiwan, ROC
[4]US Army Edgewood Chemical and Biological Center
Aberdeen Proving Ground, MD 21010
[5]ANP Technologies Inc.
824 Interchange Boulevard, Newark, DE 19711

ABSTRACT

There is an immediate need for the ability to detect, identify and quantify chemical and biological agents in water supplies during water point selection, production, storage, and distribution to consumers. Through a U.S. Army sponsored Joint Service Agent Water Monitor (JSAWM) program, based on hand-held assays that exist in a ticket format, we are developing new algorithms for automatic processing of tickets. In previous work, detection of control dots in the tickets was carried out by traditional image segmentation approaches such as Otsu's method and other entropy-based thresholding techniques. In experiments, it was found that the approaches above were sensitive to illumination effects in the camera reader. As a result, more robust, object-oriented approaches to detect the control dots are required. Mathematical morphology is a powerful technique for image analysis that focuses on the size and shape of the objects in the scene. In this work, we describe a novel application of morphological operations in identification of control dots in hand held assay ticket imagery. Such images were pre-processed by a light compensation algorithm prior to morphological analysis. The performance of the proposed approach is evaluated using Receiving Operating Characteristics (ROC) analysis.

Keywords: Chemical/biological agent detection. Hand held assay(HHA). Mathematical morphology. ROC analysis.

1. INTRODUCTION

Hand-held assay (HHA) is a form of biological assay which is designed to provide a quick and accurate presumptive identification of selected biological warfare agents. The HHA works on the principle of antigen/antibody interactions[1]. An antigen is any foreign substance that, when introduced into the host, are capable of eliciting an immune response, which ultimately results in antibody production. Antibodies are molecules that are produced in response to a given antigen. Biologically, the role of the antibody is to bind the intruding foreign substance and facilitate its removal from the body. The HHA exploits the sensitivity and specificity of antibodies to detect and differentiate antigens. The results provided by the HHA can be utilized to advise and assist in facilitating the resolution of a biological incident. It is only after an agent's identity can be ascertained that an effective outer perimeter can be established, neutralization plans

Chemical and Biological Standoff Detection II, edited by James O. Jensen,
Jean-Marc Thériault, Proceedings of SPIE Vol. 5584 (SPIE, Bellingham, WA, 2004)
0277-786X/04/$15 · doi: 10.1117/12.571968

formulated, decontamination procedures enacted, emergency medical treatment plans made, and environmental preservation precautions taken.

Through a U.S. Army sponsored Joint Service Agent Water Monitor (JSAWM) program, we are developing new algorithms for automatic processing of HHAs that exist in ticket format. Tickets offer many unique advantages over their bulky instrument-based counterparts: they are compact, easy to use, and have no power source requirements. For instance, ANP Technologies Inc., a nano/biotechnology-based company settled in Newark, Delaware, has recently developed devices that can reliably detect the presence of biological agents in HHA tickets at extremely low concentrations. The tickets can either be read by the human eye or by an optical scanner. Although quantitative measurements using the HHAs require an optical scanner, commercially available scanners such as those used in medical image analysis are usually very expensive. Fortunately, a new method has been recently developed to collect the data using a flatbed optical scanner to scan images of tested HHAs. In an initial demonstration, the inexpensive flatbed scanner significantly outperformed commercial scanners in reading the HHAs and providing quantitative information about the amount of biological warfare simulant present in a water sample. However, to fully exploit the flatbed scanner in reading the JSAWM HHAs, new image processing algorithms must be developed.

Our main goal in this paper is to develop image processing algorithms that can be employed to automatically process HHA tickets. In order to accomplish the above goal, accurate detection of control dots in the tickets is essential since these dots provide baseline for other agent detection. In previous work, detection of control dots was carried out by traditional image segmentation approaches such as Otsu's method and other entropy-based thresholding techniques[2]. In experiments, it was found that the approaches above were sensitive to illumination effects in the camera reader. Improvements are thus needed for increasing the ability to automatically detect control dots in image tickets and decrease the background noise and illumination interferers. The above goals can help automate processing algorithms and to integrate them with the scanner and computer, so that a single untrained operator can reliably use the system. In doing so, we propose to use reconstruction-based morphological operations[3-5], which are able to accurately characterize image objects in terms of their size and shape and, therefore, can be used to detect control dots in image tickets with very high precision. The simple approach adopted in this work to reduce illumination effects is to apply a light compensation algorithm prior to morphological analysis.

The remainder of this paper is organized as follows. In Section 2, we briefly describe mathematical morphology theory, with special emphasis on reconstruction-based morphological operators that will be used thoroughly throughout the paper. Section 3 develops a custom-designed algorithm to automatically process ticket images based on morphological reconstruction operations. Section 4 summarizes experimental results after applying our algorithm to a database of 40 ticket samples provided by the ANP Technologies Inc.. In order to accurately determine the sensitivity of HHAs and reduce the risk in the JSAWM program, receiver operating characteristic (ROC) curves are constructed and thoroughly analyzed. Finally, Section 5 concludes with some remarks.

2. MATHEMATICAL MORPHOLOGY

Mathematical morphology (MM) is a theory for spatial structure that has been successfully used in various pattern recognition applications. Based on set theory, binary MM was established by introducing fundamental operators applied to two sets[3]. One set is processed by another one having a carefully selected shape and size, and known as the Structuring Element (SE), which is translated over the image. The SE acts as a probe for extracting or suppressing specific structures of the image objects, checking that each position of the SE fits within the image objects. MM operations have been extended to gray-tone images by viewing these data as an imaginary topographic relief[4]; in this regard, the brighter the gray tone, the higher the corresponding elevation. It follows that, in grayscale morphology, each $2-\mathrm{D}$ gray tone image is viewed as if it were a digital elevation model (DEM). In practice, set operators directly generalize to gray-tone images. For instance, the intersection $\cap$ (respectively, union $\cup$) of two sets becomes the point-wise minimum $\wedge$ (respectively, maximum) operator. In a similar way to the binary case, specific image structures are extracted/suppressed according to the chosen SE. The latter is usually "flat" in the sense that it is defined in the spatial domain of the image (the x-y plane). Therefore, classic MM looks for objects defined as a specific spatial arrangement of pixels.

2.1 Classic morphological operations

The two basic operations of classic MM are dilation and erosion. Following a usual notation[5], let us consider a grayscale image f, defined on a space E. Typically, E is the 2-D continuous space R^2 or the 2-D discrete space Z^2. In the following, we refer to morphological operations defined on the discrete space. The flat erosion of f by $B \subset Z^2$ is defined by the following expression:

$$(f \otimes B)(x,y) = \bigwedge_{(s,t)\in Z^2(B)} f(x+s, y+t), \qquad (x,y)\in Z^2, \tag{1}$$

where $Z^2(B)$ denotes the set of discrete spatial coordinates associated to pixels lying within the neighborhood defined by B and $\bigwedge$ denotes the minimum. On the other hand, the flat dilation of f by B is defined by

$$(f \oplus B)(x,y) = \bigvee_{(s,t)\in Z^2(B)} f(x-s, y-t), \qquad (x,y)\in Z^2, \tag{2}$$

where $\bigvee$ denotes the maximum. For illustrative purposes, let B be a flat disk SE with radius of 14 pixels, and let f be a HHA ticket image from the ANP database, pre-processed by a combined noise removal and light compensation technique [see Fig. 1(a)]. As can be examined in Fig. 1(b), morphological dilation based on a disk-shaped structuring element B has the effect of expanding dark zones (in the example, the two control dots are developed). On the other hand, morphological erosion based on B expands bright areas and shrinks dark areas [see Fig. 1(c)]. Object extension/contraction depends on the size and shape of the considered SE. As demonstrated by this example, erosion and dilation generally modify the properties of the objects in the scene.

2.2 Reconstruction-based morphological operations

Opening and closing by reconstruction are a special class of morphological filters that have proven to be very successful for multi-scale image processing[6]. These filters can accurately preserve the shapes observed in input images. Let us consider a greyscale image f defined on Z^2. Given a SE (designed by B) of minimal size, opening by reconstruction can be defined by the following expression:

$$(f \circ B)^k(x,y) = \bigvee_{k\geq 1} \left[\delta_B^k (f \circ B \mid f)\right](x,y), \tag{3}$$

where

$$\left[\delta_B^k (f \circ B \mid f)\right](x,y) = \left[\overbrace{\delta_B \delta_B \cdots \delta_B}^{k \text{ times}} (f \circ B \mid f)\right](x,y). \tag{4}$$

The elementary term $\left[\delta_B (f \circ B \mid f)\right](x,y)$ is a geodesic dilation, defined as the maximum of the elementary dilation of $f \circ B$ using B at pixel (x,y) and the value of $f(x,y)$,

$$\left[\delta_B (f \circ B \mid f)\right](x,y) = \bigvee\{[(f \circ B) \oplus B](x,y), f(x,y)\}. \tag{5}$$

As shown above, this operation is repeated *k* times until idempotence (i.e. no pixel value modifications) is reached. In similar fashion, closing by reconstruction is given by:

$$(f \bullet B)^k(x,y) = \bigwedge_{k\geq 1} \left[\varepsilon_B^k (f \bullet B \mid f)\right](x,y), \tag{6}$$

where

$$\left[\varepsilon_B^k (f \bullet B \mid f)\right](x,y) = \left[\overbrace{\varepsilon_B \varepsilon_B \cdots \varepsilon_B}^{k \text{ times}} (f \bullet B \mid f)\right](x,y). \tag{7}$$

The elementary term $\left[\varepsilon_B (f \bullet B \mid f)\right](x,y)$ is an extended geodesic erosion, defined as the minimum of the elementary erosion of $f \bullet B$ using B at pixel (x,y) and the value of $f(x,y)$,

$$\left[\varepsilon_B (f \bullet B \mid f)\right](x,y) = \bigwedge\{[(f \bullet B) \otimes B](x,y), f(x,y)\}. \tag{8}$$

In the following, we use closing by reconstruction as the fundamental operation for detecting control dots in HHA water ticket images. The proposed transforms can be used to isolate bright (opening) and dark (closing) pixels in greyscale images, where the notion of bright/dark refers to the most highly bright/dark pixels among the surrounding pixels. In order to detect pure pixels, we define the extended top-hat operator, Γ, which is calculated by taking the residual image between the original and the opened image[4].

$$\Gamma[f(x,y)] = \mathrm{Dist}[f(x,y), (f \circ B)(x,y)], \tag{9}$$

where Dist is the Euclidean distance. In a similar way, the inverse extended top-hat operator, Γ', can accurately detect dark pixels according to the size and shape of the structuring element B.

$$\Gamma'[f(x,y)] = \mathrm{Dist}[(f \bullet B)(x,y), f(x,y)]. \tag{10}$$

3. AUTOMATIC MORPHOLOGICAL TICKET PROCESSING ALGORITHM (AMTPA)

This section develops an automatic algorithm for morphological processing of HHA tickets, which is based on the morphological operations addressed in the previous section. Before describing the algorithm, we must first note that a pre-processing stage is required in order to remove noise and illumination effects in the images acquired by the camera reader. The former goal is accomplished by using a simple 3x3 median filter. In order to deal with the latter problem, we have further developed an adaptative technique that estimates how much light should be compensated for each pixel in the image. Here we briefly describe the procedure followed to estimate the amount of light compensation from both vertical and horizontal directions. For the vertical direction, we simply average the gray level values of the pixels in columns 20^{th} and 200^{th} and subtract each element of the resulting vector from the maximum gray level in the scene. As a result, a light level compensation pattern in the vertical direction is obtained. A similar approach is applied to produce a light level compensation pattern in horizontal orientation. In this case, we average the gray level values of the pixels in rows 5^{th}, 10^{th}, 15^{th}, and 20^{th} and then subtract each element of the resulting vector from the maximum gray level in the scene.

With the above pre-processing techniques in mind, we describe next the proposed algorithm for automatic processing of HHA image tickets. The images were collected using a flatbed scanner with resolution of 200 dpi. The size of the images is 640x480 pixels with dynamic range of 8 bits (256 gray levels). In what follows, we assume that the ticket window in each HHA image has been cropped from the image, a task that can be easily accomplished by a simple edge detection algorithm. With the above assumption in mind, the step-by-step algorithmic description of an automatic morphological ticket processing algorithm (AMTPA) is given below:

AMTPA algorithm

1. Pre-processing:
    1.1. Apply a 3x3 smoothing filter to remove noise from the cropped ticket window.
    1.2. Estimate vertical and horizontal light patterns in the HHA ticket window and obtain the corresponding light compensation masks.

1.3. Remove the shadow effects from the control dot region by applying the light compensation masks above [see Fig. 1(a)].

2. Identification of control dots:
   2.1. Apply a morphological inverse top-hat operator to the image resulting from step 2.2 [see Fig. 1(e)].
   2.2. Apply Otsu's automatic segmentation method to the image resulting from step 2.3 [see Fig. 1(f)].
3. Positioning the geographical center of the control dots and antigen dots:
   3.1. Calculate the centroid of the two control dots.
   3.2. Estimate the approximate location of antigen dots, i.e. 200 pixels from the centroid of the control dots and 110 pixels from each antigen [see Fig. 1(g)].
4. Estimating the concentration of each antigen in the antigen dots:
   4.1 Extract the gray level value at the corresponding antigen dot pixel locations.
   4.2 Use a lookup table that relates the gray level value at each antigen's dot pixel location with the concentration of each antigen in the ticket.

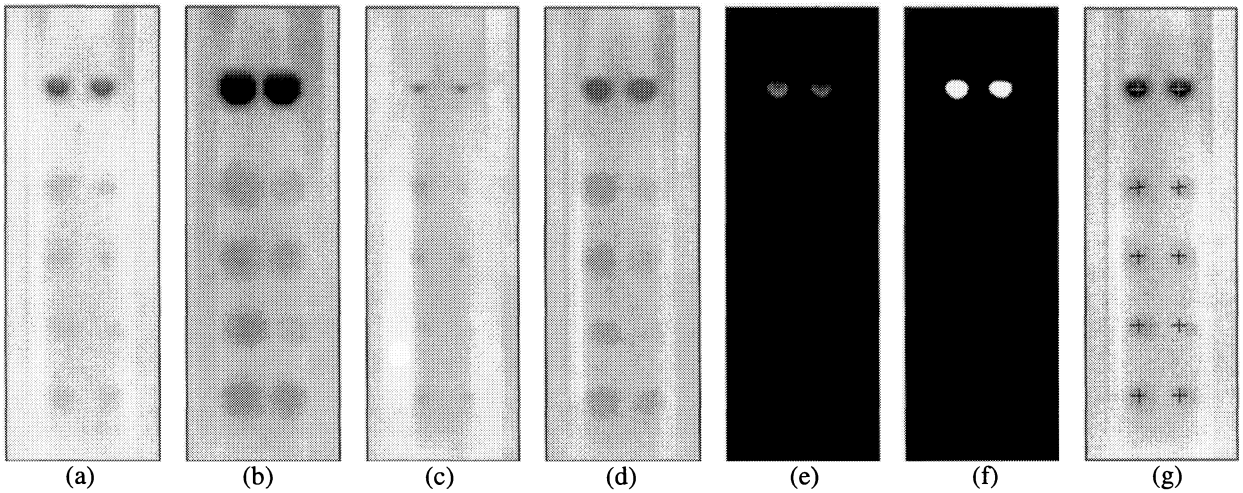

Figure 1. Morphological processing of a HHA ticket image. (a) Original image pre-processed by noise removal and light compensation. (b) Eroded image. (c) Dilated image. (d) Image after closing by reconstruction. (e) Image after inverse top-hat operator. (f) Segmentation by Otsu's method. (g) Identification of control dots in the original image.

Morphological by reconstruction presents important advantages over traditional morphological operations. First, if the searched patterns do not have regular properties across the scene, an adaptative scheme is needed to ensure that the correct SE size and shape is considered at each pixel. This need consequently poses the problem of adequate parameter selection and multi-scale image processing, which can be successfully accomplished by opening and closing by reconstruction. Second, these filters do not introduce discontinuities and therefore preserve very accurately the objects in the original image. In order to illustrate the reconstruction-based operations addressed above, let f be the HHA ticket image in Fig. 1(a). Similarly, let B be a flat disk SE with radius of 14 pixels. The size and shape of the considered SE has been selected according to the spatial properties of the objects of interest in the scene, in this case, the two control dots at the top of the ticket window area. As displayed in Fig. 1(d), a closing by reconstruction operation based on B produces an image which is similar to the original image in Fig. 1(a). However, it should be noted that the two control dots have been smoothed so that their contrast with regard to the background is more diffuse than in Fig. 1(a). If we now apply a morphological inverse top-hat operator, which is calculated by taking the residual image between the original image in Fig. 1(a) and the image in Fig. 1(d), the resulting image [see Fig. 1(e)] provides a clear separation between the objects of interest (i.e. the two control dots) and the image background. In this case, the control dots have been detected and separated from the image background by means of the considered SE, whose size and shape accurately match those of the two control dots of interest. Finally, a simple automatic segmentation method such as Otsu's method[2] can easily extract the two control dots from Fig. 1(e), as displayed in Fig. 1(f).

4. EXPERIMENTAL RESULTS

In this section, we summarize the results obtained after applying our AMTPA algorithm to a database of 40 HHA ticket images with ground-truth antigen concentrations provided by the ANP. A major question arising in our detection application is how can we objectively evaluate whether or the proposed technique is effective and in what sense. Receiver Operating Characteristics (ROC) analysis has been widely used for that purpose[7]. Before addressing our experimental results, we first provide a description of the use of ROC analysis in the considered application.

4.1 ROC analysis

The goal of traditional ROC analysis is to plot a curve, referred to as ROC curve, based on the detection probability (P_D) versus false alarm probability (P_F). This curve focuses on the effectiveness of a decision made for a detection problem, regardless of what specific criterion should be used. In order to develop ROC curves in our particular application, we need to calculate P_D and P_F of each antigen m_j for $j = 1,...,4$ in the HHA ticket image, where the m_j can be given by different combinations of antigens such as vaccinia, coxiella, ricin or bot tow[1]. Setting a concentration threshold for each antigen to be detected is an important task in chemical and biological applications, where the presence of a threat usually depends on whether its concentration or abundance is above a certain tolerance threshold. If the concentration is greater than the threshold, we claim that the antigen is detected. Otherwise, we consider that no antigen is detected. Let t be the detection threshold value used as a desired cutoff threshold value. Similarly, let $g_{m_j}(x, y)$ be the gray level value that is proportional to the concentration of antigen m_j at the pixel with spatial location (x,y) detected in the ticket image. Using t as a detection threshold value we can define a detector, denoted by d_t by

$$d_t(g_{m_j}(x, y)) = \begin{cases} 1, & \text{if } g_{m_j}(x, y) \geq t \\ 0, & \text{if } g_{m_j}(x, y) < t \end{cases} \tag{11}$$

which uses t as a threshold value to convert a gray level value $g_{m_j}(x, y)$ to a binary value. Accordingly, a "1" produced by Eq. (11) indicates that antigen m_j is detected at pixel at spatial location (x,y) in the HHA ticket image; otherwise, we consider that antigen m_j is not present at (x,y). The detection rate $R_D(m_j)$ and the false alarm rate $R_F(m_j)$ are defined by

$$R_D(m_j) = \frac{N_D(m_j)}{N(m_j)}, \tag{12}$$

$$R_F(m_j) = \frac{N_F(m_j)}{N - N(m_j)}, \tag{13}$$

where $N_D(m_j)$ is the total number of pixels in which the presence of antigen m_j is correctly detected, $N_F(m_j)$ is the total number of pixels in which the presence of m_j is detected as a false alarm, $N(m_j)$ is the total number of pixels which contain m_j, and N is the total number of pixels in the ticket image. From Eqs. (11-13), it is clear that each fixed t produces a point in a 2-D ROC curve given by $(R_D(m_j),R_F(m_j))$ for the antigen m_j. Now, if we vary t in a third dimension, it results in a 3-D ROC curve[8-9] for m_j where $(R_D(m_j),t)$ can be plot versus $R_F(m_j)$. Using this 3-D curve we can further plot three 2-D curves, a curve of $R_D(m_j)$ versus $R_F(m_j)$ which is the traditional ROC curve, a curve of $R_D(m_j)$ versus t, and a curve of $R_F(m_j)$ versus t for performance analysis. Finally, the mean detection rate $\overline{R}_D$ and mean false alarm rate $\overline{R}_F$ can be further defined by

$$\overline{R}_D = \sum_{j=1}^{4} p(m_j) R_D(m_j), \tag{14}$$

$$\overline{R}_F = \sum_{j=1}^{4} p(m_j) R_F(m_j), \tag{15}$$

where $p(m_j) = N(m_j) \Big/ \sum_{j=1}^{4} N(m_j)$. Similarly, each fixed t also produces a point in a 2-D ROC curve given by $(\overline{R}_D, \overline{R}_F)$. By varying the detection threshold value t in a third dimension, it also results in a 3-D mean-ROC curve, which can be used to evaluate the performance of the proposed detection algorithm by plotting $(\overline{R}_D, t)$ versus $\overline{R}_F$. Using this 3-D mean-ROC curve we can further plot three 2-D ROC curves, a curve of $\overline{R}_D$ versus $\overline{R}_F$ which is the traditional ROC curve, a curve of $\overline{R}_D$ versus t, and a curve of $\overline{R}_F$ versus t for detection performance analysis. Once the 2-D ROC curve of $(\overline{R}_D, \overline{R}_F)$ is generated, the area under the curve is calculated and defined as overall detection rate (DR), which can be used to evaluate the effectiveness of the proposed detector. So, when the DR is 1, the detector can be considered an ideal detector. Conversely, when DR is 0.5, the detector performs the worst.

4.2 Results and discussion

In this subsection we conduct an investigation of the performance of the AMTPA algorithm based on 3-D and 2-D ROC analysis addressed in the previous subsection. As shown in Fig. 2, the 3-D ROC curve in Fig. 2(a) shows the performance of the AMTPA as a function of three parameters, $\overline{R}_D$, $\overline{R}_F$ and t. While the 2-D ROC curve of $(\overline{R}_D, \overline{R}_F)$ in Fig. 2(b) provides the mean detection rate of the AMTPA versus the mean false alarm rate, the 2-D ROC curves of $(\overline{R}_D, t)$ and $(\overline{R}_F, t)$ in Fig. 2(c-d) indicate how a threshold value of t affects the performance of the AMTPA.

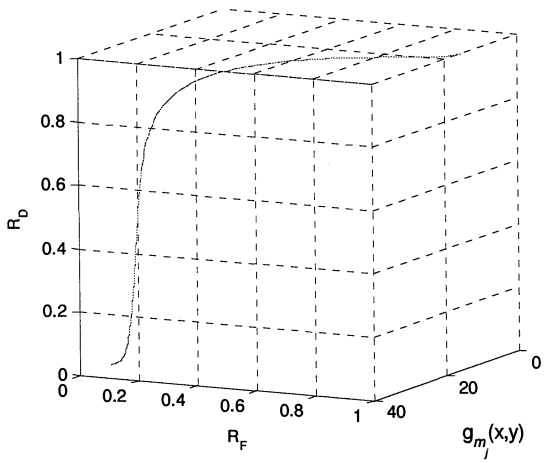

(a) 3-D ROC curve of $(\overline{R}_D, \overline{R}_F, t)$

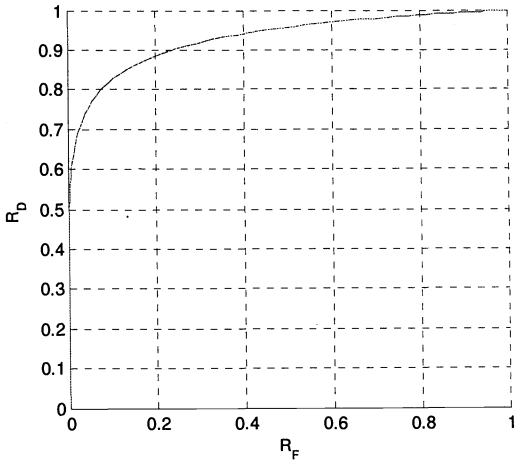

(b) 2-D ROC curve of $(\overline{R}_D, \overline{R}_F)$

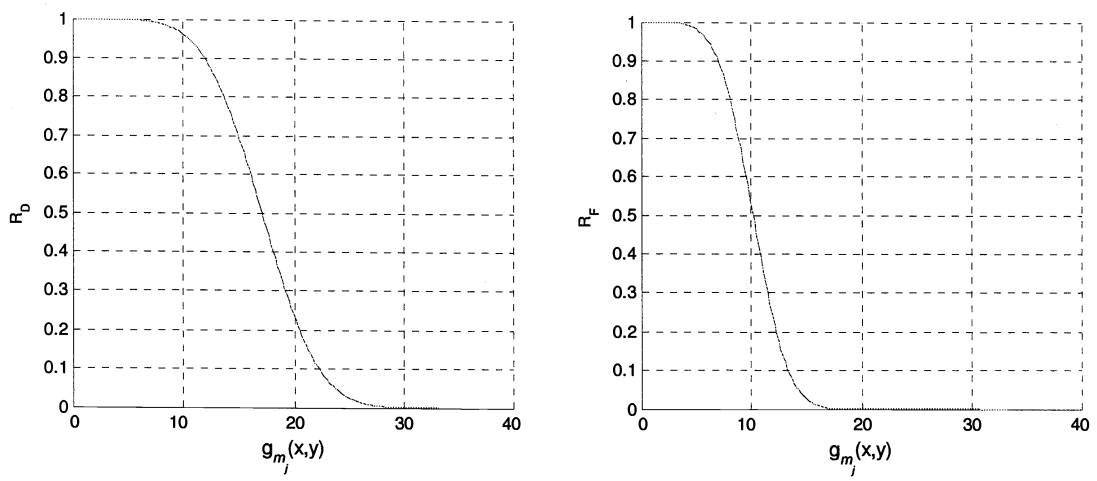

(c) 2-D ROC curve of $(\overline{R}_D, t)$

(d) 2-D ROC curve of $(\overline{R}_F, t)$

Figure 2. (a) 3-D ROC curve of $(\overline{R}_D, \overline{R}_F, t)$; (b) 2-D ROC curve of $(\overline{R}_D, \overline{R}_F)$; (c) 2-D ROC curve of $(\overline{R}_D, t)$;(d) 2-D ROC curve of $(\overline{R}_F, t)$.

It should be noted that the mean detection rate (DR) can be simply obtained by calculating the area under the 2-D ROC curve in Fig. 2(b). By looking at the 3-D ROC curve in Fig. 2(a), it is clear that the proposed algorithm is able to produce high scores of $\overline{R}_D$ and low scores of $\overline{R}_F$ for different values of t. Specifically, Fig. 2(b) reveals that the 2-D ROC curve of $(\overline{R}_D, \overline{R}_F)$ is close to optimal. The higher the ROC curve, the better the detection power. The worst case is the one which produces the diagonal line, in which case $\overline{R}_D$ and $\overline{R}_F$ yield the same probability, i.e. $1/2$ and, subsequently, $DR = 0.5$. That would imply that the method is completely useless since it would be equivalent to flipping a coin to make the decision without designing any technique at all. In order to measure the detection power of our proposed AMTPA algorithm, we have calculated the area under the 2-D ROC curve in Fig. 2(b), which resulted in $DR = 0.85$. This indicated that the proposed algorithm could be successfully used to detect the presence of a biological threat in HHA ticket imagery. According to Fig. 2(c), the $\overline{R}_D$ of the proposed AMTPA algorithm dropped to zero for a small concentration. This demonstrated that the $\overline{R}_D$ of the proposed algorithm is sensitive to a small concentration t of an antigen, which is of great interest in the considered biological application where sensitivity to concentration of a certain antigen is the key element in order to determine if the considered antigen represents a threat or not. Similar phenomena were also observed in the 2-D curve of $(\overline{R}_F, t)$ [see Fig. 2(d)], where in this case $\overline{R}_F$ dropped drastically around $t = 5$.

5. CONCLUSIONS AND FUTURE RESEARCH

Hand held assay (HHA) is a form of biological assay that represents a powerful technique designed to provide a quick and accurate identification of selected biological warfare agents. Although HHAs are fairly reliable, accurate and sensitive assaying of environmental samples is exceedingly difficult. Automatic processing of HHAs is highly desirable in order overcome potential deficiencies/limitations that may arise in the analysis process, usually carried out by a trained operator. This paper has developed a fully automatic algorithm for detection and quantification of chemical and biological agents on HHAs that exist in a ticket format. In order to accurately determine the sensitivity of the HHAs and reduce the risk in the advanced acquisition system, 3-D ROC analysis was conducted on a data set made up with 40 ticket image samples with ground-truth antigen concentrations, provided by the ANP Technologies Inc. The proposed 3-D ROC analysis takes advantage of concentrations produced by our proposed detector, and then thresholds these concentration estimates. By adjusting the percentage of concentration of an antigen we can calculate the detection rate

and false alarm rate for performance analysis, which is crucial in chemical and biological standoff detection applications where the presence of a threat generally depends on whether its concentration is above a specified tolerance threshold. Experimental results reveal that the proposed algorithm can automatically detect the exact location of antigen dots in the ticket images with great accuracy, and further estimate the concentration of each antigen in the corresponding dots. Future research will focus on testing the proposed algorithm with additional samples provided by the ANP and exploring additional methods for reliable estimation of antigen concentrations.

ACKNOWLEDGEMENT

The authors would like to thank the Army Research Office to support this work. Antonio Plaza would like to thank for support received from the Spanish Ministry of Education and Science (PR2003-0360 Fellowship).

REFERENCES

1. P. A. Emanuel, J. Dang, J. S. Gebhardt, J. Aldrich, E. A. E. Garber, H. Kulaga, P. Stopa, J. J. Valdes and A. Dion-Schultz, "Recombinant antibodies: a new reagent for biological agent detection," *Biosensors and Bioelectronics*, vol. 14, pp. 751-759, 2000.
2. P. K. Sahoo, S. Soltani, and A. K. C. Wong, "A survey of thresholding techniques," *Comput. Vision, Graphics Image Processing*, vol. 41, pp. 233–260, 1988.
3. J. Serra, *Image analysis and mathematical morphology*. London: Academic Press, 1982.
4. P. Soille, *Morphological image analysis: Principles and applications*, 2nd Edition, Springer Verlag, Berlin, 2003.
5. A. Plaza, P. Martinez, R. Perez and J. Plaza, "Spatial/spectral endmember extraction by multidimensional morphological operations," *IEEE Transactions on Geoscience and Remote Sensing,* vol. 40, pp. 2025-2041, 2002.
6. M. Pesaresi and J.A. Benediktsson, "A new approach for the morphological segmentation of high-resolution satellite imagery," *IEEE Transactions on Geoscience and Remote Sensing,* vol. vol.39, pp.309-320, 2001.
7. H. V. Poor, *An introduction to signal detection and estimation*, Springer-Verlag, 1988.
8. C.-I Chang, *Hyperspectral imaging: spectral detection and classification*, Kluwer Academic/Plenum Publishers, New York, 2003.
9. C.-I Chang, "Target signature-constrained mixed pixel classification for hyperspectral imagery," *IEEE Transactions on Geoscience and Remote Sensing*, vol. 40, pp. 1065-1081, 2002.